Brain Stimulation 19 (2026) 103034

Contents lists available at ScienceDirect

Brain Stimulation

journal homepage: www.journals.elsevier.com/brain-stimulation

Modulation of motor cortical theta and gamma oscillations using phase-targeted, closed-loop optogenetic stimulation of local excitatory and inhibitory neurons

Jessica L. Myatt [a,b,2], Robert Toth [a,b,c,2], Timothy Denison [a,b,c], Isaac Grennan [a,b], Colin G. McNamara [a,d,e], Charlotte J. Stagg [a,b,f,*,1], Andrew Sharott [a,b,**,1]

[a] Medical Research Council Brain Network Dynamics Unit, Nuffield Department of Clinical Neurosciences, University of Oxford, Oxford, United Kingdom
[b] Medical Research Council Centre of Research Excellence in Restorative Neural Dynamics, United Kingdom
[c] Department of Engineering Science, University of Oxford, Oxford, United Kingdom
[d] Department of Physiology, School of Medicine, College of Medicine and Health, University College Cork, Cork, Ireland
[e] APC Microbiome Ireland, University College Cork, Cork, Ireland
[f] Centre for Integrative Neuroimaging, FMRIB, Nuffield Department of Clinical Neurosciences, University of Oxford, United Kingdom

A B S T R A C T

Theta and gamma oscillations are prominent features of cortical local field potentials (LFPs) and stimulation of the motor cortex at these frequencies can enhance motor learning. Phase-targeted closed-loop stimulation could provide a more precise and effective method to modulate these oscillations, particularly if stimulation parameters could harness the dynamics of the specific circuit mechanisms underpinning the generation of these activities.

To investigate this, we defined the response of theta- and gamma-frequency oscillations in the motor cortex to closed-loop optogenetic stimulation of excitatory pyramidal neurons and inhibitory interneurons transfected with Channelrhodopsin-2 in awake, head-fixed RBP4-Cre (retinol-binding-protein-4) and PV-Cre (parvalbumin) mice, respectively. Phase-targeted blue-light pulses were delivered using the OscillTrack algorithm to track theta phase in the cortical LFP in real time and trigger stimulation at one of four target theta phases. Stimulation was delivered over a quarter of the target theta cycle, either as a single continuous pulse ("continuous" protocol) or three short pulses at gamma (75Hz) frequency ("gamma" protocol).

Stimulation of both neuron types, using either stimulation protocol, modulated theta power in a phase-dependent manner, with continuous stimulation of excitatory neurons leading to stronger modulation. Phase-dependent amplification during stimulation of excitatory vs inhibitory neurons was offset by 90°, in line with predictions from computational models. Replay of previously recorded closed-loop stimulation patterns in an open-loop configuration failed to reproduce the same phase-specific effects, highlighting the necessity of real-time closed-loop interaction to achieve precise modulation. Additionally, stimulation of pyramidal neurons using the gamma protocol selectively amplified gamma power, independently of the target theta phase.

These findings demonstrate that phase-dependent amplification of cortical theta power can be induced through targeted stimulation of local excitatory or inhibitory neurons, with the observed phase offset likely reflecting underlying circuit dynamics. This approach provides a framework for developing more effective brain stimulation strategies aimed at modulating oscillatory activity in humans.

1. Introduction

Oscillatory activity in the cortex emerges from the dynamic interplay between excitatory pyramidal neurons and inhibitory interneurons, which together produce a fluctuating excitatory–inhibitory balance that tightly regulates spiking activity within cortical circuits [1–4]. These processes play key roles in orchestrating information processing, communication, and coordination across large-scale neural networks, contributing to cognition, perception, memory, and motor control. Moreover, abnormalities in oscillatory activity have been implicated in numerous neurological and neuropsychiatric disorders [5]. Interventions capable of correcting these disruptions may offer a powerful

* Corresponding author. Medical Research Council Brain Network Dynamics Unit, Nuffield Department of Clinical Neurosciences, University of Oxford, Oxford, United Kingdom.
** Corresponding author. Medical Research Council Brain Network Dynamics Unit, Nuffield Department of Clinical Neurosciences, University of Oxford, Oxford, United Kingdom.
E-mail addresses: charlotte.stagg@ndcn.ox.ac.uk (C.J. Stagg), andrew.sharott@bndu.ox.ac.uk (A. Sharott).
[1] These authors contributed equally as senior authors.
[2] These authors contributed equally as first authors.

https://doi.org/10.1016/j.brs.2026.103034
Received 30 September 2025; Received in revised form 14 January 2026; Accepted 22 January 2026
Available online 22 January 2026

therapeutic approach.

In the motor cortex, theta and gamma frequency oscillations may have specific roles in motor adaptation and learning [6]. In line with this, theta-gamma coupled transcranial alternating current stimulation (tACS) of the motor cortex can improve motor learning [7], suggesting that manipulating these activities could provide a powerful therapeutic tool. Such stimulation, however, does not take the intrinsic system dynamics into account. A more effective approach could be to couple the timing of stimulation to ongoing theta and/or gamma oscillations. Phase-targeted stimulation, where the phase of an ongoing oscillation is tracked in real time and the detection of a "target" phase is used to trigger stimulation, provides a precise and effective method to achieve this. Our previous studies, where electrical stimulation was delivered to specific phases of Parkinsonian beta [8] and hippocampal theta [9] oscillations, demonstrate the capability of this approach to both amplify and suppress the target activity. Such phase-targeted stimulation could be further improved by understanding and utilising local circuit dynamics. This is particularly relevant for cortical circuits, where the mechanisms underlying oscillations are often a function of interactions between diverse neuron types in the local microcircuit [10]. To this end, several studies have utilised phase-targeted optogenetic stimulation of specific cell types [11–16], but have not compared the effects of the same closed-loop protocol to stimulate different neuron types in the target circuit. Applying such an approach to motor cortex could provide insights into the general mechanisms underlying phase-targeted neuromodulation of motor cortical circuits and motor control, including which circuit components are the key drivers. Given the ubiquitous presence of theta and gamma oscillations across cortical circuits [6,17,18], developing closed-loop stimulation protocols that target these oscillations may provide powerful tools for modulating a wide range of cortical functions.

In this study, we applied the same phase-targeted closed-loop stimulation protocols to two neuronal populations in the motor cortex of awake, head-fixed mice. Optogenetic excitation using Channelrhodopsin-2 was applied to excitatory pyramidal neurons in Layer V and parvalbumin-expressing (PV) inhibitory interneurons, using viral transfection in RBP4-Cre (retinol-binding-protein-4) and PV-Cre mice respectively. Stimulation was delivered at one of four target phases of the ongoing theta oscillation using two protocols: either a continuous pulse or a burst of gamma frequency stimulation. Stimulation of both cell types, using either stimulation protocol, resulted in phase-dependent modulation of the amplitude of ongoing motor cortical theta oscillations, but that the amplifying phase differs across the neuron types. We further demonstrate that stimulation of excitatory neurons evokes changes in gamma power more effectively. These findings provide new insights into circuit-level mechanisms shaping motor cortical oscillations, thereby informing strategies for more effective targeted therapeutic neuromodulation using non-invasive or deep brain stimulation approaches.

2. Materials & methods

2.1. Animals

All studies were performed in accordance with institutional guidelines and the Animal (Scientific Procedures) Act, 1986 (United Kingdom). Experimental procedures were conducted in adult mice (male) either B6; 129P2-Pvalb$^{tm1(cre)Arbr}$ (PV-Cre, heterozygous on a C57BL/BJ background (n = 11), Jackson Laboratories) or Tg(RBP4-Cre) KL100Gsat (RBP4-Cre, heterozygous with a C57BL/BJ background, Jackson Laboratories) (n = 14), weighing 23–43g. Additional mice (n = 2 PV-Cre; n = 1 RBP4-Cre) were used for verification of the immunohistochemistry protocol. Mice were kept in a 12-h light/dark cycle, with food and water provided *ad libitum*.

2.2. Surgical procedures

All surgical procedures were performed under gaseous isoflurane in oxygen anaesthesia (4 % for induction, maintained at 1–2 %). Anaesthetised mice were secured in stereotaxic apparatus (David Kopf Instruments), and body temperature was maintained at 37 ± 0.5 °C. Analgesia (Buprenorphine; 0.08 mg/kg in sterile saline) was administered subcutaneously after induction of anaesthesia. Prior to viral injection and headplate surgeries, a local anaesthetic (Marcain; 2 mg/kg) was injected into the scalp subcutaneously. Following surgical procedures, a subcutaneous injection of 0.4 ml pre-warmed isotonic glucose solution was given.

2.2.1. Viral injection

Viral expression in neurons was achieved by unilaterally injecting 100 nl of AAV5-Ef1a-DIO-ChR2(E123T/T259C)-eYFP (~6.2×10^{12} vg/ml; Deisseroth Vector Core, University of North Carolina) (ChR2) or control AAV5-Ef1a-DIO-eYFP (~4×10^{12} vg/ml; Deisseroth Vector Core) vector (which will not express ChR2) into the right motor cortex (AP +1.5 mm, ML +1.3 mm, DV +0.8 mm; from Bregma).

2.2.2. Headplate implantation

Mice were implanted with a titanium custom-made headplate (Get It Made Ltd, London) (0.7 g, internal diameter 9 mm) to enable head-fixation. Skin overlying the skull was removed, the skull was washed (3 %, H_20_2 in dH_20 followed by sterile saline), then etched for improved adhesion. Edges of skin were glued (Vetbond) to the skull, before the headplate was aligned to bregma and lambda, then bonded to the skull using clear dental cement (Super Bond C&B, Parkell), a thin layer of which was also used over the entire exposed skull surface. A craniotomy was made to insert a reference screw (Precision technology, East Grinstead) wrapped in wire over the ipsilateral cerebellum to the injection site, this was fixed with dental cement (Jet Denture Repair Power: Lang Dental, Illinois, USA; Meadway Repair Liquid: MR. Dental, Surrey).

2.2.3. Craniotomy for electrophysiological recordings

The day prior to recording, a small craniotomy (~1.5 mm^2) was made above the recording site. To provide a protective barrier over exposed brain tissue, dura gel (Cambridge NeuroTech) and silicone (Body Double, Smooth-On) were used following the surgery and between electrophysiological recordings.

2.3. Electrophysiological recordings

Electrophysiological recordings (maximum 5 per mouse) were undertaken in awake head-fixed mice previously habituated to the rig, in which the mouse sat head-fixed in a cardboard tube, with a cork lined 3D printed insert, supported by a caddy. A faraday cage was used to shield the set-up from electromagnetic signals in the external environment.

To record local field potentials in the motor cortex (probe depth 1000–1300 μm), linear four shank 32 channel probes (100 μm between contacts, 200 μm between shanks; A4x8-100-200-177-OA32; NeuroNexus, Michigan, USA) were used for acute recordings. A cortical headstage (64-channel; Intan Technologies, California, USA) was attached to the probe using an adaptor (Adpt-A32-OM32, Omnetics, Minnesota, USA) and connector (OM32, NeuroNexus), as well as to both a grounding wire and cerebellar reference screw. All electrophysiological recordings were collected using the Intan RHD2000 system at a sampling rate of 20 kHz. The probe was positioned above the desired coordinates using a stereotaxic frame and arm (Kopf Instruments, California, USA). In later recordings, the probe had an additional 'Z-Coat' (NeuroNexus, Michigan, USA). On the second shank, 200 μm above the top contact site was an integrated optic fiber, used to deliver optogenetic stimulation (473 nm; Cobolt Laser, Sweden) via a connected optic fiber (105 μm core, 200 μm, 0.22 NA, Thorlabs, New jersey, USA). Laser power was verified and adjusted for every session using a power meter

interface (PM100USB, Thorlabs) and sphere photodiode power sensor (S140C, Thorlabs).

2.4. Theta phase locked optogenetic stimulation

Online phase tracking of 6Hz motor cortical theta was performed using the OscillTrack algorithm [19] and used to drive optogenetic stimulation at specific phases of ongoing theta activity. The real-time phase estimate was calculated in the field-programmable gate array (FPGA) of the Intan RHD2000 USB interface board, allowing target phase and stimulation output to be selected on a GUI. In each recording session a phase reference channel was selected from visual observation of baseline spiking activity. This channel was high-pass filtered using a 1st order digital filter with a corner frequency of 4Hz to reduce the interference of intense 3Hz delta activity, then down-sampled 49-fold to a rate of 408Hz for processing. The algorithm was configured with a loop-gain of 0.0625 and a centre frequency of 6Hz in all sessions. A real-time trigger was only generated at the target phase if more than 80 % of the period of the 6Hz theta cycle had passed (timeout: 133.333 ms) to reduce erroneous triggering [8]. During continuous stimulation, PV-Cre and RBP4-Cre ChR2 mice were stimulated at mean frequencies of 4.65 ± 0.57Hz and 4.83 ± 0.25Hz, corresponding to approximately 78 and 80 % of the theoretical maximum of continuous theta wave, respectively. Under gamma stimulation conditions, stimulation frequencies averaged 4.74 ± 0.25Hz (~79 %) and 4.84 ± 0.23Hz (~81 %), respectively.

2.5. Optogenetic stimulation protocols

Stimulation patterns (Table 1 & Fig. 1A–C) were delivered to the motor cortex for a period of ~2.5–7 min over four different phases of the 6Hz theta cycle, centred to the target phase, in a randomised order at a combination of different laser powers (0 mW (unstimulated control), 1 mW, and 2 mW). *Continuous* stimulation consisted of a single, uninterrupted pulse delivered for a duration of approximately 1/4 of the 6Hz theta cycle. *Gamma* stimulation consisted of 3 short pulses (each 6667μs) evenly spaced at a frequency equivalent to 75Hz (see Table 1). *Arrhythmic gamma* stimulation was used to interrogate whether gamma *rhythmicity* was necessary to produce effects seen in response to the gamma protocol. As such, the middle of the three pulses varied in position between the two outside pulses based on a set of 31 positions, leading to stimulation that delivered the same energy over the same overall time window, but without the periodic component of the main protocol. To confirm that gamma and arrhythmic gamma stimulation delivered equivalent light energy for this comparison, we verified that the number of stimulation events was closely matched, and comparable across conditions (Table S1).

To differentiate the effect of theta phase locked stimulation from the temporal pattern of optogenetic stimulation trains generated through closed-loop recordings, an 'open-loop replay' paradigm was introduced to later recording sessions (Fig. 1D and E). These were pre-recorded stimulation patterns generated during closed-loop stimulation (details as noted above) replayed using the Intan digital output files during the same recording session. Thus, the pattern of stimulation was the same, but with no relationship to the phase of the ongoing theta oscillation.

Table 1
Stimulation patterns used for closed-loop optogenetic electrophysiology.

Stim Pattern	Stim length (μs)	Pulse on (μs)	Pulse off (μs)	Timeout (μs)	Number of pulses
Gamma	33335	6667	6667	133333	3
Continuous pulse	41667	41667	0	133333	1
Arrhythmic gamma	33335	6667	Random interval	133333	3

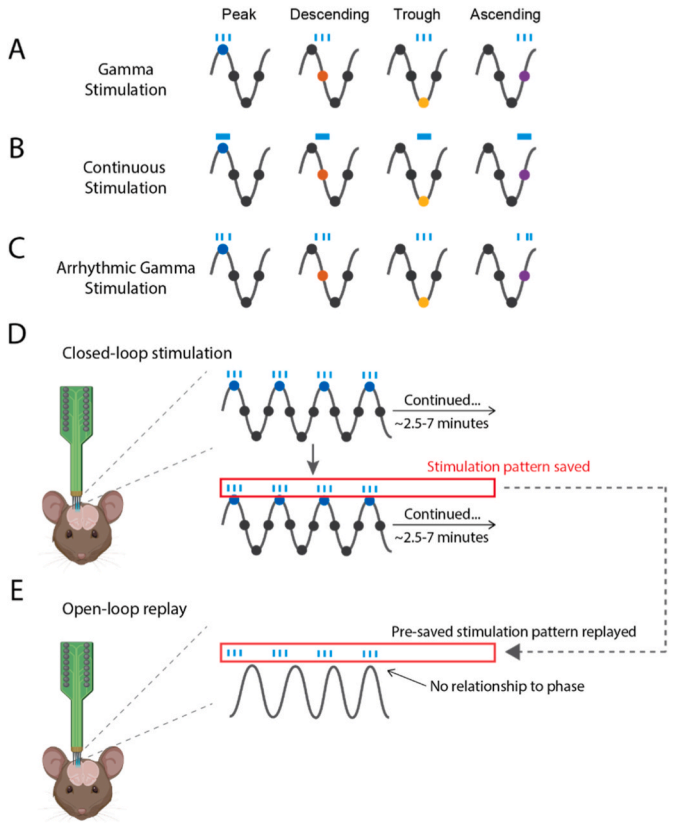

Fig. 1. Stimulation patterns and targets for phase-targeted closed-loop and open-loop replay optogenetic stimulation. (**A** & **B**) Two optogenetic stimulation patterns were devised to interrogate whether there was differential modulation over 4 different phases of the theta cycle. The first was a burst of 3 pulses at gamma frequency (75Hz) (**A**), with the middle pulse centred to the phase, and the second a simple ON/OFF pattern over ¼ of the theta cycle (41.667 ms) (**B**). In some experiments, an arrhythmic gamma protocol (**C**) was used to interrogate the importance of gamma rhythmicity in the circuit. In this protocol, the two outside pulses had the same interval as gamma stimulation, but the middle pulse was placed randomly between them resulting in 3 pulses that were spaced within the total duration of the main gamma protocol, but with random interstimulus intervals. For each recording within a session, a stimulation pattern, stimulation phase and stimulation ON (1 or 2 mW) or OFF (0 mW) were chosen in a randomised order then stimulated and recorded between ~2.5 and 7 min. (**D**) The 6Hz theta oscillation was tracked using the OscillTrack algorithm on a custom Intan RHD2000 USB interface, used for both stimulation and electrophysiological recordings. In later sessions, these specific recorded patterns were transferred to an SD card to replay them to the mouse later within the same session ('open-loop replay') (**E**). Care was taken to replay them at the correct stimulation amplitude as the original closed-loop recording (1 or 2 mW). Thus, open-loop replay stimulation delivered the same number of pulses, over same total time period and used the same stimulation pattern at the same amplitude as closed-loop sessions, but with no relationship to the ongoing theta oscillation (Figure created with the help of BioRender.com).

Files were replayed through an Arduino-compatible microcontroller (Teensy 3.6; PJRC Ltd, Sherwood, Oregon, USA) randomly, taking care to use the original laser amplitude, while triggering recording of electrophysiological data through Intan RHD2000.

2.6. Viral expression & targeting

Viral expression (GFP) was visualised histologically (see supplemental methods) in all mice (100 % of animals expressed GFP), with representative images shown in Figs. S1 and S2. Cortical layers were delineated using Necab-1 and FoxP2 immunoreactivity, which labels layers IV and VI respectively. All viral injections (100 nl) were targeted

to layer V (800 μm depth).

PV-expressing interneurons are distributed across cortical layers II-VI, with a higher proportion in deeper layers [20]. In PV-Cre mice, GFP expression showed extensive colocalization with PV immunoreactivity, confirming specific targeting of PV interneurons. Expression was strongest in deeper layers near the injection site, with limited spread into superficial layers. Expression was restricted to the right cortical hemisphere with no evidence of off-target expression (Fig. S1).

Layer V cortical pyramidal neurons predominantly express retinal-binding-protein 4 (RBP4), and RBP4-Cre driver lines reliably target this population [21,22]. In RBP4-Cre mice, GFP-labelled cell bodies were largely confined to deep cortical layers in the right cortex, particularly layer V where the viral injection was targeted, consistent with the known specificity of the mouse line (Fig. S2).

2.7. Data analysis

Welch power spectral density (PSD) estimates were calculated on down-sampled data (1 kHz). Theta power was calculated using 4000 sample Fourier transforms at a 0.25Hz resolution, while analysis of gamma power was calculated using 500 sample Fourier transforms at 2.0Hz resolution, both using Hann windows with 50 % overlap. Data were taken from channels within the expected range of impedance for a given probe type to allow exclusion of bad/broken channels (probe type 1: 1.1 ± 0.3MΩ; probe type 2: 0.01–0.08MΩ (additional Z-coating)). The four channels closest to the optic fiber were excluded from all analyses, as they were most likely to be contaminated with opto-electric artefact [23]. Power spectra were then plotted for visual inspection blinded to recording condition. Recording blocks containing fewer than 1/4 of remaining channels (<7), after accounting for the removal of the four channels containing optogenetic artefacts from all datasets, were excluded from further analysis (n = 4 sessions) as well as sessions with an abnormal power spectrum across all channels (n = 5 sessions). Single recordings with spectral artefact were additionally excluded (n = 1 recording from 1 session).

For frequency domain analyses, all power spectra computed over stimulation periods had the unstimulated baseline response subtracted to emphasise the effect of stimulation. The baseline spectrum for each channel was calculated by averaging unstimulated periods spread out throughout the session to account for drift. The baseline-subtracted spectra were first averaged across channels, then again along experimental variables (genotype, phase, amplitude) for visualisation. Subsequent, statistical comparisons focused on the mean values across specific frequency bands within the theta (4.5–7.5Hz) and gamma (56.25–93.75Hz) ranges.

To determine the accuracy of stimulation delivered in each condition, we defined the phase at which stimulation was delivered as defined by a post-hoc phase estimate that used both forward and backward information. The raw LFP signal was downsampled to a rate of 500Hz and filtered between 4.5 and 7.5Hz using a zero-phase, 4th-order Butterworth filter. The instantaneous phase was then obtained by applying the Hilbert Transform. The delivered stimulation pattern was aligned to the extracellular potential, with the post-hoc phase sampled at the temporal midpoint of stimulation events. Events too close to the beginning or end of the recording were excluded from analysis to account for confounding edge-effects introduced by filtering. For each stimulation event, the phase estimate was obtained by computing the circular mean of the instantaneous phase across all remaining channels. Phase distributions were visualised as histograms of the post-hoc phase (radians) of all stimulation events for a given target phase (Figs. S3 and S4). To account for variability in recording lengths and the number of stimulations delivered, phase distributions were normalised to percentages, such that the area under the curve sums to 100 % for each target phase. In addition, to quantify phase accuracy, we calculated the proportion of stimulation pulses that fell within a quarter theta cycle centred to our targeted stimulation phase (±45°; 1/8th of a cycle either side). This was calculated separately by phase, as well as for all phases combined by stimulation pattern and group (Tables S2–4).

2.8. Statistical analyses

Statistical analyses were undertaken using linear mixed effects (LME) models where feasible (R: 4.3.2) to allow for appropriate analysis of longitudinal data with interactions and account for possible missing values. In the case there was insufficient data for a LME model, with the caveat that we were unable to control for repetition of subjects within and between sessions, paired t-tests were used as an alternative. While data was collected at two amplitudes (1 & 2 mW), LME models demonstrated no significant differences between amplitudes in terms of the main effect of amplitude or interaction terms at any given phase in either mouse group (ChR2; control), for each mouse type (PV-Cre; RBP4-Cre). Therefore, the 1 & 2 mW data were combined into a 'stimulation on' condition. As a result, the same recording sessions contribute data that were collected for multiple amplitudes at each phase and stimulation pattern. Therefore, the number of recordings per phase may be greater than the number of sessions. For a breakdown of the numbers of animals within each group, the overall number of recording sessions, recordings per phase and total number of recordings, please refer to Tables S5–7. Generally, within each recording, a minimum of 700 stimulation events were recorded. In figure legends, the number of mice and recordings per phase are provided.

Shapiro-Wilk normality tests demonstrated non-normality of the extracted PSD estimates, so data were z-scored prior to statistical analyses. Outliers within the theta range, identified as 1.5x the interquartile range (IQR) for each subset of data were extracted and re-visually inspected. While there were no grounds for exclusion and all data was included for statistical analyses, these 'outliers' have been identified on plots accompanying statistics in a lighter colour for differentiation and were not included in plotting of boxplots. For all boxplots, grey boxes represent the IQR and median values from the data set, and the whiskers extend to minimum and maximum values calculated from their quartile ±1.5*IQR for each grouped session. Individual scatter points are session means for their respective group.

All LME models contained random effects of subject (each mouse) and date (denoting a session), to account for the variability within the data that arises from grouping of observations, as mice were used across several days and different mice were commonly recorded on the same date. This controls for variation in the random effects, while determining if there are associations between the fixed effects of the model. P-values were obtained by likelihood ratio tests and REML (restricted maximum likelihood) was set to false as ML (maximum likelihood) was used to estimate both fixed and random effects. These tests used Satterthwaite's approximation for determining degrees of freedom (DF) [24]. Under this method, numerator DF (numDF) are determined by the number of parameters associated with the fixed effect (e.g. k-1, for a factor with k levels), whereas denominator DF (denDF) are estimated from the models variance structure and therefore are not directly determined from the number of mice, sessions or recordings in the accompanying supplemental materials (Tables S5–7). To follow up significant interactions ($p < 0.05$) pairwise t-tests were undertaken using the emmeans package in R (Tukey adjustment for multiple comparisons). Cohen's d was computed for pairwise contrasts as the estimated marginal mean difference divided by the residual standard deviation of the mixed model. Full results of LME models and relevant significant pairwise contrasts are given in Supplementary Tables 8–30.

3. Results

To understand how phase-dependent stimulation modulates motor cortical theta and gamma oscillations, we developed a method for delivering optogenetic stimulation triggered by specific phases of the ongoing theta oscillation in the motor cortical LFP of awake, head-fixed

mice. Using the OscillTrack algorithm, we demonstrate reliable phase tracking of the motor cortical theta oscillation (Figs. S3 and S4; Tables S2–4). Stimulation was targeted to either PV-expressing inhibitory interneurons (PV-Cre) or Layer V excitatory pyramidal (RBP4-Cre) neurons (see Figs. S1 and S2). All statistical tests were performed using linear mixed-effects models (LMEs), unless otherwise stated (see Methods).

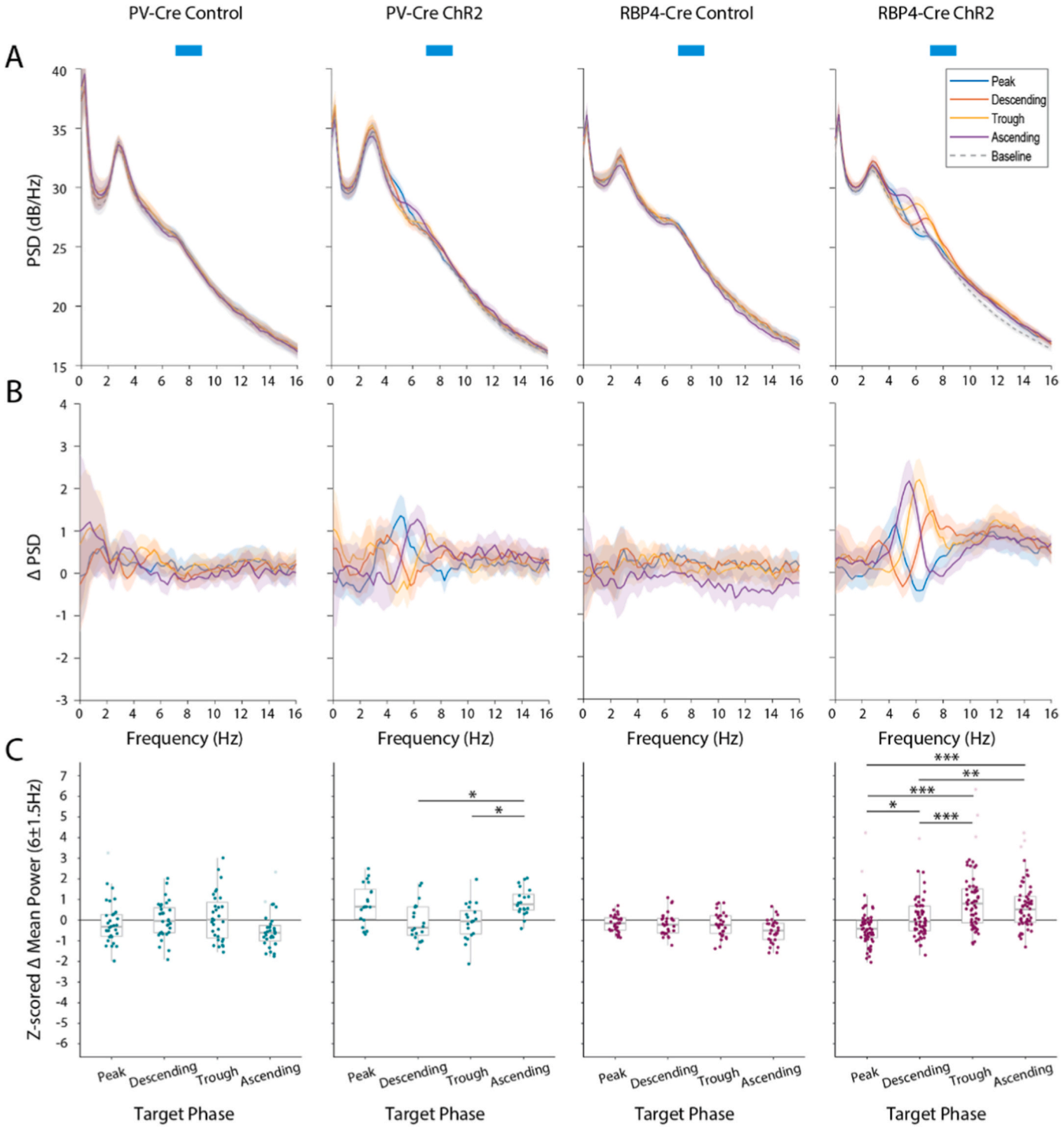

Fig. 2. Closed-loop continuous stimulation of PV+ interneurons and RBP4+ pyramidal neurons led to phase-dependent effects on local theta power. (**A**) Mean power spectral density for PV-Cre & RBP4-Cre GFP-control (n = 4 mice; 31 recordings/phase & n = 4; 30 recordings/phase respectively) and ChR2 mice (n = 5 mice; 20 recordings/phase & n = 10; 60 recordings/phase respectively), targeting 4 different phases of the theta oscillation with continuous stimulation at 1 or 2 mW. Shaded areas show ±2*SEM. (**B**) As in (A) but using baseline-subtracted spectra. (**C**) Boxplots showing the z-scored change in theta power with respect to baseline extracted between in the theta range (4.5–7.5Hz). Horizontal lines with asterisks indicate significant differences in theta power between different target phases using LME, followed by pairwise post hoc t-tests with Tukey adjustment at $p < 0.05$.

3.1. Phase-dependent modulation of the motor cortical theta power by theta-phase targeted continuous optogenetic stimulation

We first evaluated the effect of theta-phase targeted, continuous closed-loop optogenetic pulses ("continuous pulse") on the power of the ongoing theta oscillation (Fig. 2). Optogenetic stimulation can be confounded by indirect effects of the applied light [25]. To ensure that effects were dependent on opsin-mediated activation of neuronal activity, we used control animals that had been injected with a construct that transfected Cre-dependent GFP, but not the opsin (GFP-control). In opsin-transfected mice, we also compared real stimulation sessions to sessions when stimulation was turned off (i.e. the phase is tracked, but stimulation is not applied [STIM-ON and STIM-OFF]), using the time-points where stimulation *would* have occurred as the reference frame for analysis. We tested for significant main effects of group (ChR2 vs GFP-control), phase (peak, descending, ascending, and trough), stimulation (STIM-ON and STIM-OFF) and all interaction terms.

Stimulation of inhibitory interneurons using closed-loop continuous pulses led to significant phase-dependent modulation of theta power in ChR2 mice compared to GFP-controls (group*phase: $F(3,288) = 5.03$, p

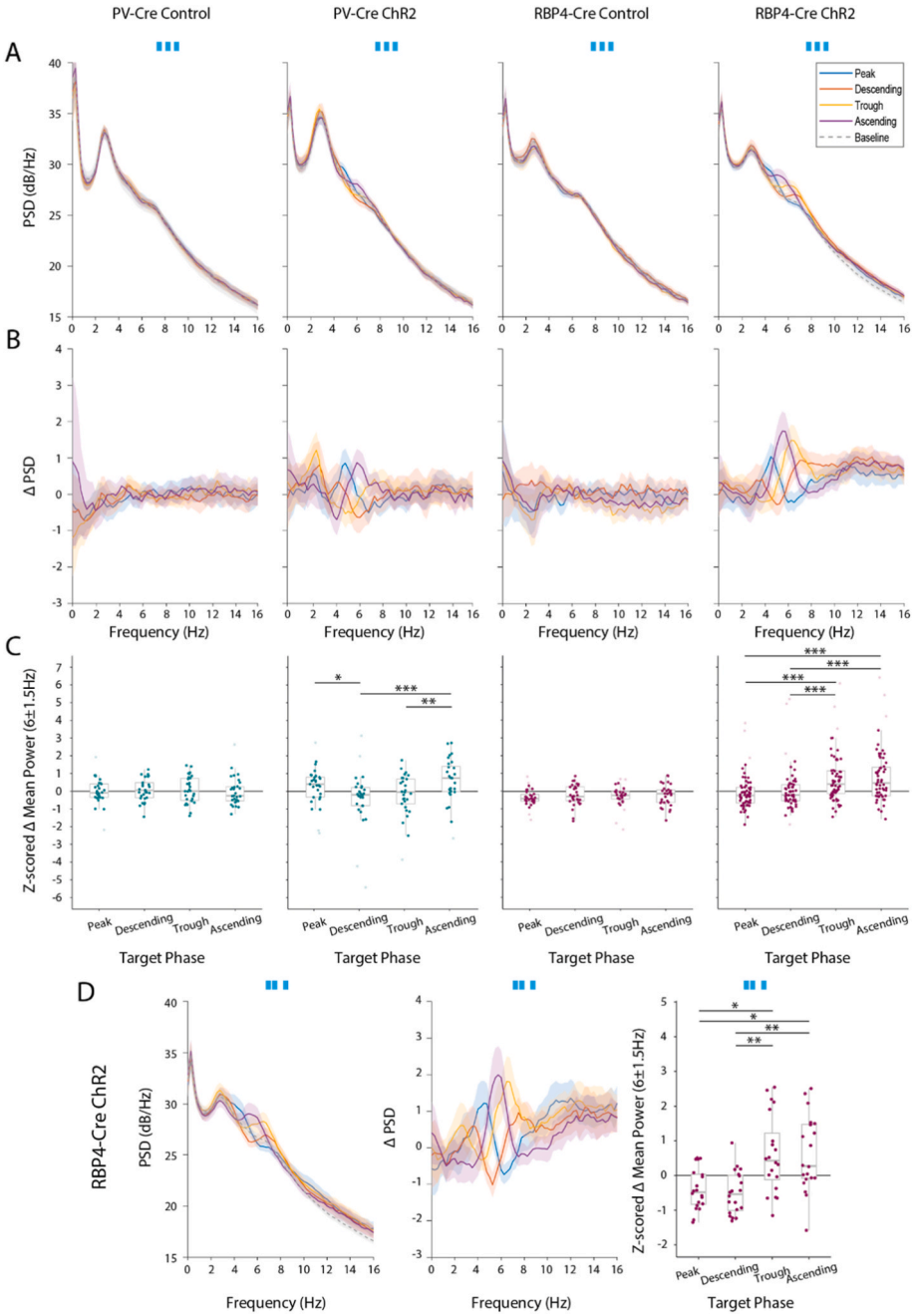

Fig. 3. Closed-loop gamma stimulation of PV+ interneurons and RBP4+ pyramidal neurons lead to phase-dependent effects on local theta power. (**A**) Mean power spectral density for PV-Cre & RBP4-Cre GFP-control (n = 4 mice; 29–30 recordings/phase & n = 4; 30 recordings/phase respectively) and ChR2 mice (n = 7 mice; 28–29 recordings/phase & n = 10; 60 recordings/phase respectively) targeting 4 different phases of the theta oscillation with gamma stimulation at 1 or 2 mW. Shaded areas show ±2*SEM. (**B**). As in (A) but using baseline-subtracted spectra. (**C**) Boxplots with the z-scored change in theta power with respect to baseline extracted between in the theta range (4.5–7.5Hz). Horizontal lines with asterisks indicate significant differences in theta power between different target phases using LME, followed by pairwise post hoc t-tests with Tukey adjustment at $p < 0.05$. (**D**) As in A-C, but for RBP4 ChR2 mice (n = 5; 20 recordings/phase) receiving arrhythmic gamma stimulation (2 mW).

= 0.002; for full statistical analyses see Table S8; Fig. 2 and Fig. S5, left), and was only present under STIM-ON conditions (stimulation: F(1,288) = 4.82, p = 0.029). Because we were primarily interested in stimulation-driven effects, we tested phase dependence only under STIM-ON conditions (group, phase and their interaction - Table S9). This demonstrated significant phase-dependent modulation of theta power in ChR2 mice compared with GFP-controls (group*phase: F(3,184) = 9.07, p < 0.001). Post hoc tests revealed significant differences in theta power across multiple phases in PV-Cre ChR2 mice, but not in GFP-controls (pairwise t-tests, Tukey adjustment for multiple comparisons; Fig. 2C left, Table S10).

In comparison, when stimulating excitatory neurons with the continuous protocol in RBP4-Cre ChR2 mice, there was a significant three-way interaction between group, phase and stimulation (F(3,469) = 6.70, p < 0.001; Table S11; Fig. 2, and Fig. S5, right). Analysis of STIM-ON data showed that ChR2 expression was necessary for phase-dependent modulation of theta power (group*phase: F(3,323) = 14.93, p < 0.001; Table S12). Subsequent pairwise t-tests identified significant differences in theta power across multiple target phases in RBP4-Cre ChR2 mice, but not in the RBP4-Cre GFP-controls (Fig. 2C, right; Table S13).

3.2. Phase-dependent modulation of the motor cortical theta power with theta-phase targeted gamma-frequency optogenetic stimulation

Given the important role of theta-gamma coupling in the motor cortex [6,7,17], we hypothesised that gamma frequency optogenetic stimulation - a burst of three pulses at 75 Hz ("gamma pulse") - might modulate theta power more effectively than the continuous pulse (Fig. 3). In PV-Cre mice, group and phase had significant effects on theta power (group*phase: F(3,324) = 4.29, p = 0.006) during closed-loop gamma pulse stimulation (Table S14; Fig. 3 and Fig. S6, left). For STIM-ON data, we identified the same significant interaction (group*phase: F(3,205) = 6.31, p < 0.001; Table S15) and post hoc tests confirmed significant phase-dependent differences in theta power in PV-Cre ChR2 mice (pairwise t-tests Tukey adjustment, Table S16; Fig. 3C, left).

Gamma pulse stimulation of excitatory neurons also led to significant modulation of theta power dependent on group and phase (group*phase: F(3,554) = 2.65, p = 0.048). As expected, theta modulation varied with stimulation condition, but only in RBP4+ ChR2 mice (group*stimulation: F(1,545) = 25.45, p < 0.001; Table S17; Fig. 3 and Fig. S6, right). We therefore performed an LME model for just the STIM-ON data (Table S18). A significant group*phase interaction (F(3,324) = 5.82, p < 0.001) indicated that ChR2 was required for phase-dependent theta modulation. Subsequent pairwise t-tests (Tukey adjustment for multiple comparisons) identified significant differences in theta power across multiple target phases (Fig. 3C, right; Table S19).

To determine the importance of rhythmicity of gamma pulse stimulation on modulation of theta power in RBP4-Cre ChR2 mice, we tested a control stimulation pulse without the oscillatory component of the stimulus ("arrhythmic gamma"). For this control protocol, the middle pulse was pseudorandomly placed between the two outer pulses. Thus, the total number of pulses and mean intervals between pulses were identical to gamma pulse stimulation, but without gamma rhythmicity. Stimulation counts and thus overall light delivery were comparable between patterns (Table S1). We tested the effects of stimulation pattern (gamma pulse, arrhythmic gamma), stimulation (ON, OFF), phase (peak, descending, trough and ascending) and all combinations of interactions (Table S20). There were no effects of stimulation pattern on phase-dependent theta power modulation (stimulation pattern*phase: F(3,299) = 0.61, p = 0.609), suggesting that the rhythmic component of the pulses was not necessary to modulate theta power. Supporting this finding, a comparison of all three optogenetic stimulation patterns in the STIM-ON data revealed no significant interaction terms (Table S21). Follow-up pairwise t-tests (Tukey adjustment for multiple comparisons) identified significant differences between theta power at multiple phases following arrhythmic gamma frequency stimulation (Fig. 3D–Table S22). Overall, these results show that while bursts of optogenetic pulses applied over a specific phase of the theta cycle were sufficient for phase-dependent modulation of theta power, a periodic gamma pulse was not necessary to achieve these effects.

3.3. Closed-loop interaction is necessary for phase-dependent effects on theta power

Altering the target phase of closed-loop stimulation can produce different rates and patterns of stimulation pulses, due to the continuous interaction between the neural signal and stimulus output [8], Fig. S3. These primary statistical features of the stimulation trains could result in different effects between target phases. As we have done previously, to ensure phase-dependent theta modulation resulted from the interaction between the closed-loop system and the neural oscillation, we used an open-loop replay paradigm whereby the stimulation patterns generated by closed-loop stimulation at each target phase were "played back" in the same session they were recorded [8,9] (Fig. 1E, Fig. S4). Open-loop replay stimulation did not reproduce the phase-specific effects observed during closed-loop recordings in RBP4-Cre or PV-Cre ChR2 mice (Fig. 4, Figs. S7 and S8). We compared the z-scored difference in mean theta power between the phases with the greatest and least amplification during closed-loop stimulation and matched open-loop counterparts in RBP4-Cre ChR2 mice (LME: Stimulation type; gamma frequency: F(1, 65) = 89.65, p < 0.001, Fig. 4D left; continuous pulse: F(1,42) = 50.27, p < 0.001, Fig. 4D, right). The LME for gamma frequency including random effects for both subject and date resulted in a singular fit, with the subject variance estimated at ~0. Model comparison confirmed that including subject in this instance did not improve fit and as such date was included as the only random effect for this analysis. When the datasets for these recordings in RBP4-Cre and PV-Cre ChR2 mice were too small for LME models, the same data were compared using paired t-tests following arrhythmic gamma (t(11) = 4.81, p < 0.001 (Fig. S7D)) in RBP4-Cre, and gamma (t(11) = 3.66, p < 0.01) and continuous stimulation (t(12) = 5.02, p < 0.001 (Fig. S8D, left & right respectively)), in PV-Cre ChR2 mice.

3.4. Closed-loop stimulation of cortical pyramidal neurons leads to greater amplification of gamma power than PV-expressing interneurons

Theta and gamma oscillations are often coupled in cortical circuits and gamma-frequency stimulation has previously been shown to modulate gamma-band power. [17,26–29]. We next investigated whether our stimulation protocols also modulated gamma-frequency oscillations (Fig. 5; Figs. S9–12). Mean power spectra in the gamma range for different target phases using both gamma (Fig. 5 & Fig. S9, S10) and continuous (Figs. S11–12) stimulation were tightly overlaid, suggesting minimal effect of theta-phase targeting on gamma modulation. In line with this observation, we found no significant effects of target theta phase in any of the stimulation protocols (Tables S23–26).

As there was no phase-dependence, we combined data across target phases to examine the effects of different stimulation protocols on gamma power. We first tested for significant effects of group (PV-Cre (ChR2, GFP-control) and RBP4-Cre mice (ChR2, GFP-control)) and stimulation (ON, OFF), alongside their interaction term for each stimulation pattern (gamma (Table S27); continuous (Table S28)). Both gamma (group*stimulation: F(3,861) = 50.14, p < 0.001; Table S27, Fig. 5, Figs. S9 and S10) and continuous pulse (group*stimulation: F(3,751) = 7.93, p < 0.001; Table S28, Figs. S11–12) stimulation protocols modulated gamma power, although continuous stimulation did not lead to the same clear peak in the gamma range (Fig. S11). Post hoc tests confirmed a significant difference between gamma pulse stimulation in ON vs OFF conditions in the ChR2 group (Fig. 5, Fig. S9), for both PV-Cre (t(865.2) = -3.051, p = 0.048, Cohen's d = 0.501) and RBP4-Cre

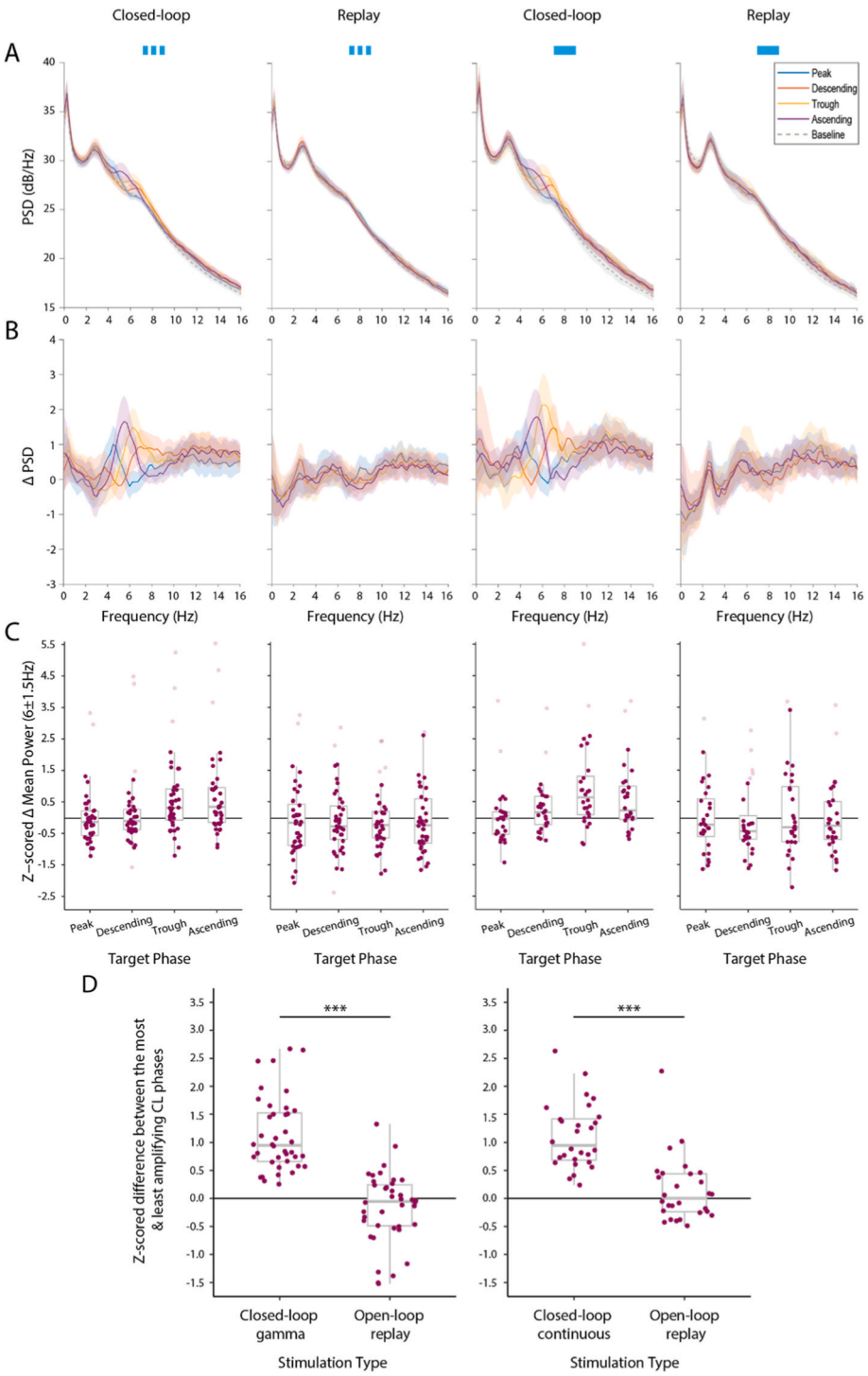

Fig. 4. Closed-loop interaction is necessary in producing the same theta phase-dependent effects following both gamma and continuous optogenetic stimulation. (A) Mean power spectral density in RBP4-Cre ChR2 mice with gamma (n = 9 mice; 40 recordings/phase) or continuous (n = 4 mice; 28 recordings/phase) at 1 or 2 mW using closed-loop and open-loop replay (replay) protocols. Shaded areas show ±2*SEM. **(B)** As in (A) but using baseline-subtracted spectra. **(C)** Boxplots with the z-scored change in theta power with respect to baseline extracted between in the theta range (4.5–7.5Hz). **(D)** For each main stimulation pattern (gamma - left/continuous - right) the difference between the most and least amplifying phase for a closed-loop recording are plotted as individual scatter points, the difference between the same phases is then taken in the open-loop recording and displayed as individual scatter points. Significant differences (*$p < 0.05$) were found between the z-scored difference in theta power of the most and least amplifying phases in each specific closed-loop recording and their open-loop counterpart for both gamma and continuous stimulation (LME, main effect: stimulation type).

mice ($t(866.3) = -20.385$, $p < 0.001$, Cohen's $d = 2.113$) (Fig. 5E). However, while there was a significant effect of gamma stimulation in the STIM-ON condition between RBP4-Cre ChR2 and GFP-controls ($t(29.4) = -4.675$, $p = 0.001$, Cohen's $d = 1.737$), this was not the case for PV-Cre ChR2/GFP-controls ($t(39.3) = -0.322$, $p > 0.05$) (Fig. 5, Fig. S10). This suggests that gamma modulation in PV-Cre animals was not mediated by stimulation and/or opsin activation. Post hoc tests only identified a significant difference in gamma power following continuous

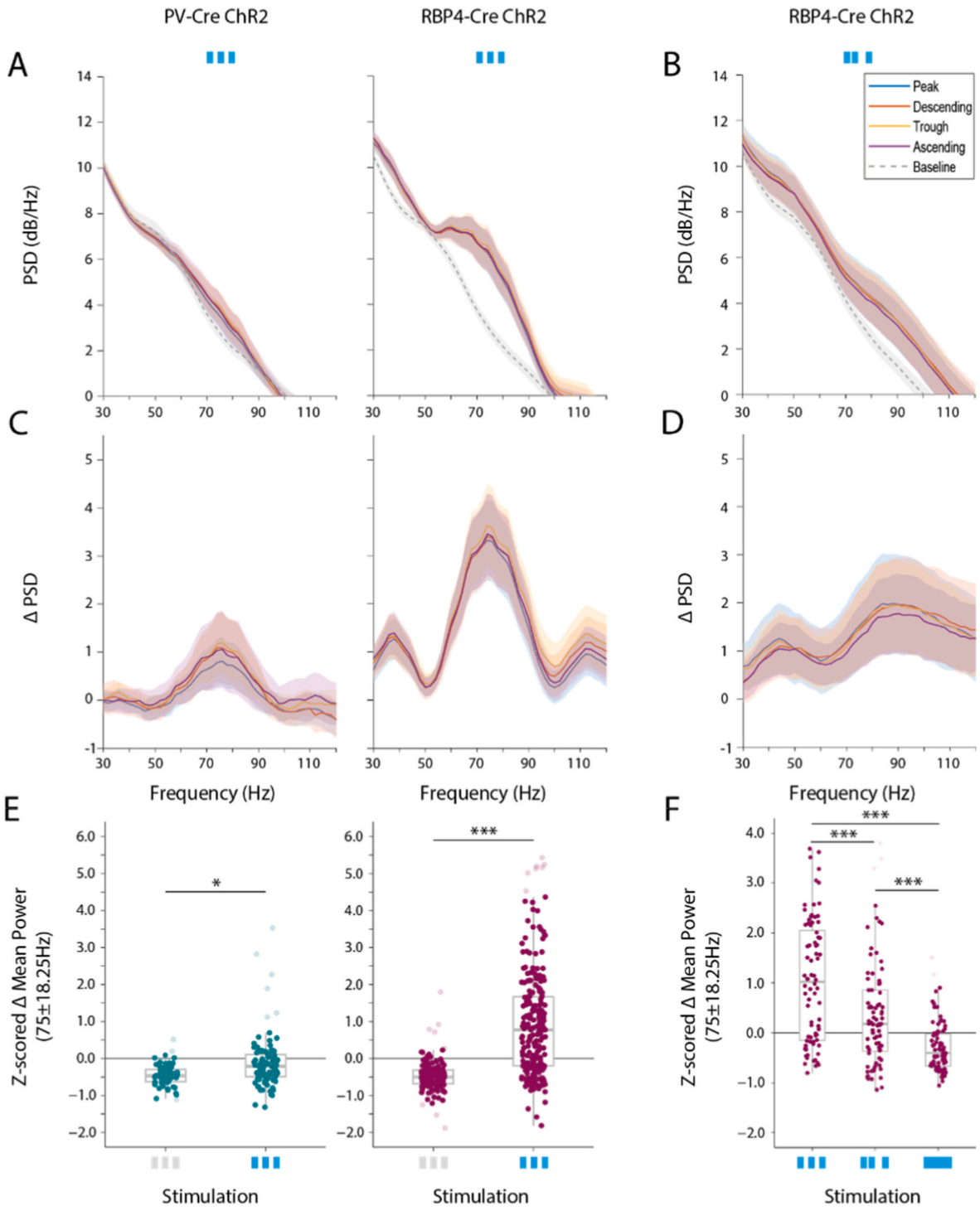

Fig. 5. Closed-loop gamma stimulation of PV+ interneurons and RBP4+ pyramidal neurons led to no phase-dependent effects on local gamma power. (A) Mean power spectral density from 30 to 120Hz for PV-Cre ChR2 (n = 6 mice; 26–27 recordings/phase) and RBP4-Cre ChR2 (n = 10; 60 recordings/phase) mice, targeting four different phases of the theta oscillation with gamma stimulation at 1 or 2 mW. Shaded areas show ±2*SEM. **(B)** Mean power spectral density from 30 to 120Hz for RBP4-Cre ChR2 mice receiving arrhythmic gamma stimulation (n = 5; 20 recordings/phase) at 2 mW. **(C–D)** As in (A–B) but using baseline-subtracted spectra. **(E)** Statistical analyses performed demonstrated no significant main effect or interaction terms including phase on gamma power (all $p > 0.05$; LME), subsequently, data from all phases was combined for further analyses. Boxplots with the z-scored change in mean gamma power with respect to baseline extracted between in the gamma band (56.75–93.25Hz) for PV-Cre and RBP4-Cre ChR2 mice during gamma stimulation (1 or 2 mW) vs no stimulation. Gamma power was significantly higher when stimulation was on in both PV-Cre and RBP4-Cre mice (*$p = 0.048$ & $p < 0.001$ respectively, LME – significant group*stimulation interaction; followed by pairwise post hoc t-tests with Tukey adjustment). **(F)**. Z-scored change in mean gamma power in RBP4-Cre mice was significantly different between all three stimulation patterns (2 mW only; *$p < 0.001$ LME followed by pairwise post hoc t-tests with Tukey adjustment).

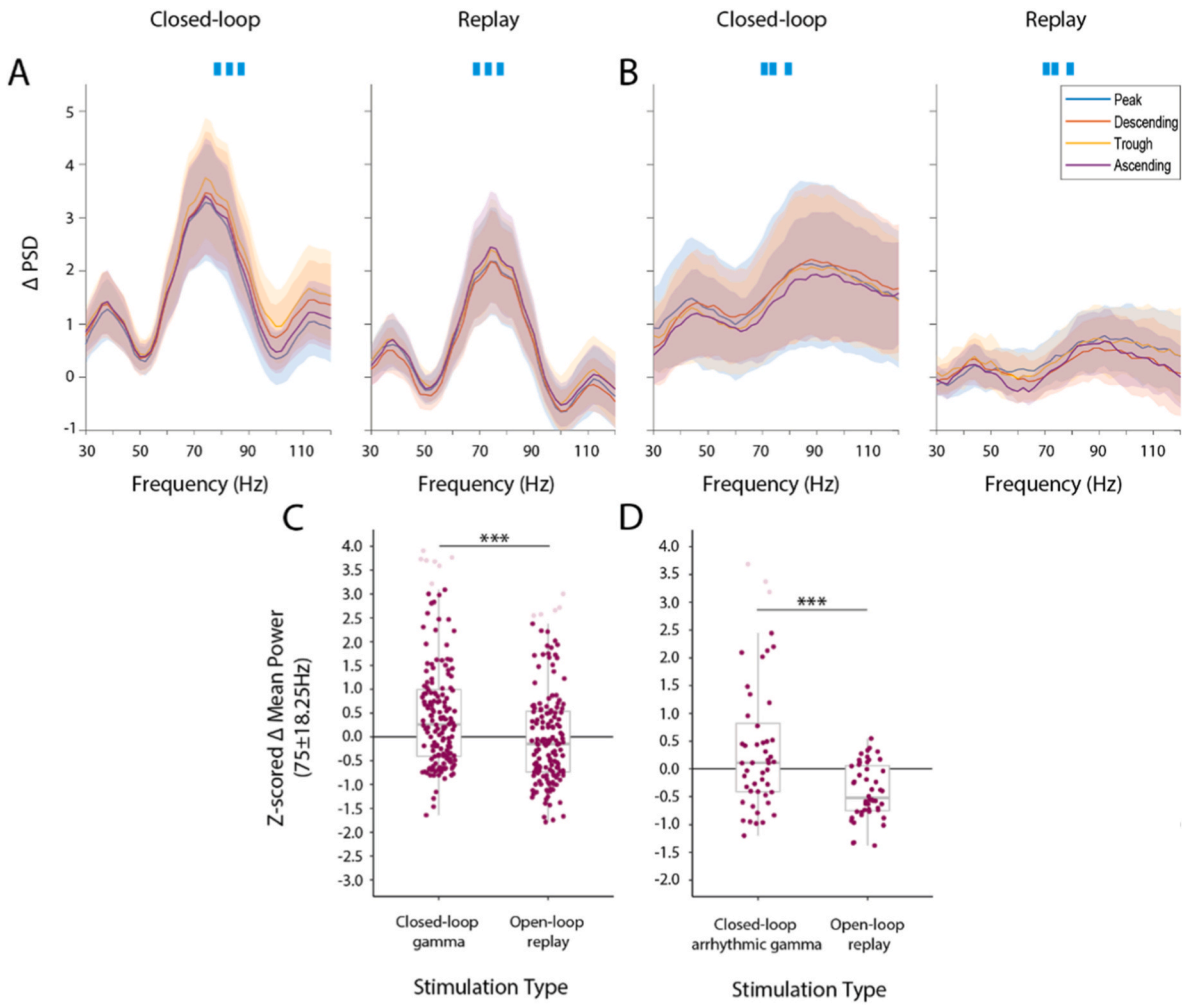

Fig. 6. Closed-loop interaction increases gamma amplification in RBP4-Cre mice. (**A**) Baseline-subtracted mean power spectral density from 30 to 120Hz in RBP4-Cre ChR2 mice receiving closed-loop gamma (n = 9 mice; 40 recordings/phase, 160 total recordings; 1 or 2 mW) or arrhythmic gamma (n = 5; 12 recordings/phase, 48 total recordings; 2 mW only) using both closed-loop and open-loop replay protocols. **(C–D)** Boxplots demonstrate z-scored change in gamma power with respect to baseline extracted between our target range of 56.75–93.25Hz (75Hz ± 18.25). Gamma power was significantly higher during closed-loop protocols for both gamma and arhythmic gamma stimulation ($p < 0.001$ (LME model: group (ChR2, control)*stimulation type (closed-loop, replay) followed by pairwise post hoc t-tests with Tukey adjustment & LME: stimulation type, respectively)).

stimulation (ON versus OFF) in RBP4-Cre ChR2 mice ($t(785.9) = -7.145$, $p < 0.001$, Cohen's $d = 0.936$; Fig. S11C). Overall, gamma stimulation of excitatory neurons was the most effective way to drive gamma power in the LFP. Moreover, in RBP4-Cre ChR2 mice, arrhythmic gamma stimulation was significantly less effective in modulating gamma power (LME model: stimulation pattern (gamma, arrhythmic gamma & continuous) - $F(2,227) = 62.75$, $p < 0.001$). Follow-up post hoc tests revealed significant differences among all stimulation patterns (all $p < 0.001$, Table S29; Fig. 5F). While the rhythmicity of the gamma pulse did not affect the modulation of theta power, it did therefore affect the amount of gamma amplification.

3.5. Theta-phase locking increases amplification of gamma power, but not in a phase-dependent manner

We hypothesised that if theta-phase targeting has no effect on gamma amplification, open-loop replay should have equivalent effects to closed-loop stimulation on this parameter. Using the gamma pulse protocol in RBP4-Cre mice, we found that this was not the case; gamma power modulation was stronger for closed-loop stimulation than open-loop replay of the same patterns (Fig. 6). This was revealed by a significant effect of group (ChR2, control) by stimulation type (closed-loop, open-loop replay) interaction ($F(1,453) = 15.67$, $p < 0.001$; Table S30) followed by pairwise post hoc t-tests with Tukey adjustment which identified a significant difference in ChR2 mice (gamma vs replay, $t(455.0) = 7.954$, $p < 0.001$, Cohen's $d = 0.891$) (Fig. 6C). A similar result was found for arrhythmic gamma stimulation (main effect of stimulation type LME; $F(1,88) = 33.04$, $p < 0.001$; Fig. 6D) in ChR2 mice. In summary, both closed-loop phase targeting and the rhythmicity of the gamma pulse influenced amplification of gamma power by our stimulation protocols.

4. Discussion

Here we demonstrate that closed-loop, theta phase-targeted optogenetic stimulation of inhibitory interneurons and excitatory pyramidal neurons in the mouse motor cortex results in phase-dependent enhancement of theta power. Gamma-pulse stimulation was sufficient to modulate theta power, despite considerably less energy being applied during the target phase of stimulation. In addition, delivery of the higher energy, continuous stimulation during the open-loop replay paradigm was not sufficient to modulate theta power. Overall, the temporal alignment of stimulation pulses, rather than their total energy, was the key factor in determining power modulation. However, delivering

gamma-pulse stimulation at higher amplitudes, to match the total power of the continuous protocol, may lead to greater overall modulation of theta power. The closed-loop interaction was necessary for producing theta modulation, which was not reproduced by replaying the same stimulation patterns uncoupled from ongoing activity. Stimulating pyramidal neurons with gamma pulses led to the largest amplification of gamma power. While the amplification of gamma modulation was not theta-phase dependent, it was greater during phase-targeted/closed-loop stimulation *per se*. Overall, we demonstrate the feasibility and effectiveness of this method for exploring the mechanisms underlying the response of cortical microcircuits to closed-loop stimulation paradigms.

4.1. Theta power is amplified at different target phases for stimulation of pyramidal neurons and interneurons

To date, studies on phase-targeted stimulation have either used electrical stimulation or have targeted a single neuron type with optogenetics. Neither of these approaches provides insight into how different components of the underlying neural circuits respond to the same closed-loop strategy. Our work reveals an offset of 90° between our two target neuronal populations in the stimulation phases that amplify theta oscillations. Maximal amplification of theta occurred when stimulating interneurons and excitatory neurons at the ascending/peak and the trough/ascending LFP phases, respectively. This finding aligns with predictions from computational models exploring perturbations of excitatory and inhibitory circuits [30]. Moreover, studies targeting gamma oscillations in the hippocampus and prefrontal cortex have shown that peak firing phase of pyramidal neurons precedes that of interneurons [31–34]. Identifying how individual neurons in these different populations respond to closed-loop stimulation will provide further insight as to how the microcircuit responds to these approaches.

Alongside phase-dependent amplification, frequency shifts in theta were observed when targeting both inhibitory and excitatory cell types. This may result from a constant phase-reset of the theta oscillation, in which an oscillation alters its timing to synchronise with the external stimulus [35,36]. Ultimately, whether optogenetic stimulation advances or delays the theta oscillation appears to depend on the phase targeted. The magnitude of a phase-reset has also been found to depend on oscillatory amplitude, as well as input strength, where lower oscillatory power can lead to larger phase resets [36–38]. This aligns with the larger frequency shift (~1Hz) observed when targeting interneurons where the amplitude is less modulated, in comparison to pyramidal neurons, which show a smaller frequency shift (~0.5Hz). In contrast to our previous studies [8,9], we were unable to bidirectionally modulate theta in this study. This could partly be due to the low baseline amplitude of the motor cortical theta power, leaving only a small lower dynamic range available for suppression.

4.2. Stimulation of pyramidal neurons led to greater amplification of gamma power

Contrary to previous studies highlighting a role of parvalbumin containing interneurons in the generation and maintenance of gamma oscillations [26,27,39], stimulation of excitatory neurons was more effective in amplifying gamma power. More specifically, rhythmic gamma stimulation (75Hz) of excitatory, but not inhibitory, neurons led to significant enhancement of gamma oscillations compared to GFP-controls. This is supported by Nicholson and colleagues (2018) [12] who demonstrated bidirectional modulation of gamma oscillations through optogenetic stimulation of pyramidal cells, but not interneurons, *in vitro*. They proposed that this resulted from out-of-phase recruitment of interneurons, which strongly suppressed the oscillation [12] as a direct result of desynchronisation. This mechanism could potentially explain our findings in a head-fixed, non-behaving context, where spontaneous gamma is low. Theta phase locked stimulation of PV+ interneurons may impose powerful network inhibition on local excitatory neurons, narrowing the window for effective firing and supressing generation of gamma. Therefore, stimulation-induced amplification of gamma power may be masked by circuit-level interactions. Consistent with this interpretation, Cardin et al. (2009) demonstrated gamma oscillations require rhythmic excitatory drive [26], which may further explain why theta-phase stimulation of layer V pyramidal neurons can effectively promote gamma generation. In addition, Sohal and colleagues (2009) found optogenetic stimulation of pyramidal neurons evoked gamma oscillations that are strongly phase-locked to the stimulation [27]. Our study has the potential to add to this line of research as further analyses of unit data could directly determine the extent of gamma oscillatory phase locking for individual cell types. Together, these mechanisms suggest that cortical gamma power may be more effectively driven through stimulation of excitatory neurons.

4.3. Concluding remarks

In summary, our work demonstrates the potential of phase-locked optogenetic stimulation to precisely modulate microcircuit-level mechanisms underlying specific oscillatory dynamics. This approach can be utilised to inform development of brain stimulation methods through underlying processes that modulate these activities under pathological conditions in humans.

4.4. Limitations of the study

While head-fixed preparations enable precise control over recording and stimulation conditions, by definition they inherently limit movement. Given that our recordings were in motor cortex, responses to stimulation could differ under conditions where spontaneous and/or goal-directed movements occur. In human studies, increased theta activity has been associated with movement suppression [40,41], which may align with the presence of theta when movement is suppressed in a head-fixed condition in mice. Accordingly, baseline theta power in this context likely reflects a movement-supressed, resting motor cortical state. In contrast, increases in gamma power have been observed during motor preparation and movement [42–44] and may therefore be reduced under head-fixation. During active behaviour, elevated gamma power could interact with theta-phase-dependent mechanisms, potentially further shaping network responses and revealing a role for theta-gamma coupling. In general, it is possible that motor cortical phase and amplitude responses would change in different behavioural states, as demonstrated in other contexts [9,45]. As a result, this study does not fully capture the dynamic modulation or complexity of these oscillations or potential interactions under well-defined movement conditions.

Additionally, optogenetic stimulation can induce photoelectrical artefacts, tissue heating effects, and non-specific neuronal responses that may lead to unintended false positive results [25,46–48]. We have carefully controlled for such effects using control mice, non-stimulation conditions, and low laser powers. Nevertheless, we cannot completely rule out the influence of such artefacts in our LFP recordings.

Finally, while we were successful in using closed-loop optogenetics to manipulate the motor cortical theta oscillation, there are obvious constraints in translating these methods to humans. However, closed-loop optogenetics can play a key role in informing and advancing future therapeutics, elucidating the role of different neurons in microcircuit function.

CRediT authorship contribution statement

Jessica L. Myatt: Writing – review & editing, Writing – original draft, Visualization, Methodology, Investigation, Formal analysis, Conceptualization. **Robert Toth:** Writing – review & editing, Software,

Methodology, Formal analysis, Data curation. **Timothy Denison:** Supervision, Funding acquisition. **Isaac Grennan:** Writing – review & editing, Formal analysis. **Colin G. McNamara:** Writing – review & editing, Methodology. **Charlotte J. Stagg:** Writing – review & editing, Supervision, Resources, Project administration, Funding acquisition, Conceptualization. **Andrew Sharott:** Writing – review & editing, Writing – original draft, Supervision, Resources, Project administration, Funding acquisition, Conceptualization.

Funding statement

This work was supported by the Medical Research Council awards MC_UU_00003/6 (to A.S), MC_UU_00003/3 (to T.D) and UKRI/MR/B000936/1 and Wellcome Trust awards 224430/Z/21/Z (to C.J.S) and 209120/Z/17/Z (to C.G.M).

Declaration of competing interest

C.G.M. and A.S. are inventors on an awarded patent (US12329532B2) related to the subject matter of this paper. No other competing interests to declare.

Appendix A. Supplementary data

Supplementary data to this article can be found online at https://doi.org/10.1016/j.brs.2026.103034.

References

[1] Adrian ED, Matthews BHC. The berger rhythm: potential changes from the occipital lobes in man. Brain 1934;57:355–85. https://doi.org/10.1093/BRAIN/57.4.355.
[2] Buzśaki G, Wang XJ. Mechanisms of gamma oscillations. Annu Rev Neurosci 2012;35:203–25. https://doi.org/10.1146/ANNUREV-NEURO-062111-150444.
[3] Shu Y, Hasenstaub A, McCormick DA. Turning on and off recurrent balanced cortical activity. Nature 2003;423:288–93. https://doi.org/10.1038/nature01616.
[4] Isaacson JS, Scanziani M. How inhibition shapes cortical activity. Neuron 2011;72:231–43. https://doi.org/10.1016/J.NEURON.2011.09.027.
[5] Uhlhaas PJ, Singer W. Abnormal neural oscillations and synchrony in schizophrenia. Nat Rev Neurosci 2010;11:100–13. https://doi.org/10.1038/nrn2774.
[6] Spooner RK, Wilson TW. Cortical theta–gamma coupling governs the adaptive control of motor commands. Brain Commun 2022;4. https://doi.org/10.1093/BRAINCOMMS/FCAC249. fcac249.
[7] Akkad H, Dupont-Hadwen J, Kane E, Evans C, Barrett L, Frese A, et al. Increasing human motor skill acquisition by driving theta-gamma coupling. eLife 2021;10. https://doi.org/10.7554/eLife.67355.
[8] McNamara CG, Rothwell M, Sharott A. Stable, interactive modulation of neuronal oscillations produced through brain-machine equilibrium. Cell Rep 2022;41:111616. https://doi.org/10.1016/J.CELREP.2022.111616.
[9] Grennan I, Perry B, Verghese A, Jones M, Härmson O, McNamara CG, et al. Phase-dependent closed-loop deep brain stimulation of the fornix provides bidirectional manipulation of hippocampal theta oscillations. Brain Stimul 2025;18:993–1003. https://doi.org/10.1016/J.BRS.2025.04.019.
[10] Sohal VS. Insights into cortical oscillations arising from optogenetic studies. Biol Psychiatry 2012;71:1039–45. https://doi.org/10.1016/j.biopsych.2012.01.024.
[11] Siegle JH, Wilson MA. Enhancement of encoding and retrieval functions through theta phase-specific manipulation of hippocampus. eLife 2014;3. https://doi.org/10.7554/ELIFE.03061.001.
[12] Nicholson E, Kuzmin DA, Leite M, Akam TE, Kullmann DM. Analogue closed-loop optogenetic modulation of hippocampal pyramidal cells dissociates gamma frequency and amplitude. eLife 2018;7:e38346. https://doi.org/10.7554/ELIFE.38346.
[13] Clarke-Williams CJ, Lopes-dos-Santos V, Lefèvre L, Brizee D, Causse AA, Rothaermel R, et al. Coordinating brain-distributed network activities in memory resistant to extinction. Cell 2024;187:409–427.e19. https://doi.org/10.1016/j.cell.2023.12.018.
[14] Gava GP, Lefèvre L, Broadbelt T, McHugh SB, Lopes-Dos-Santos V, Brizee D, et al. Organizing the coactivity structure of the hippocampus from robust to flexible memory. Science 2024;385:1120–7. https://doi.org/10.1126/SCIENCE.ADK9611. 1979.
[15] Kanta V, Pare D, Headley DB. Closed-loop control of gamma oscillations in the amygdala demonstrates their role in spatial memory consolidation. Nat Commun 2019;10:1–14. https://doi.org/10.1038/s41467-019-11938-8.
[16] Zaaimi B, Turnbull M, Hazra A, Wang Y, Gandara C, McLeod F, et al. Closed-loop optogenetic control of the dynamics of neural activity in non-human primates. Nat Biomed Eng 2023;7:559–75. https://doi.org/10.1038/s41551-022-00945-8.
[17] Canolty RT, Edwards E, Dalal SS, Soltani M, Nagarajan SS, Kirsch HE, et al. High gamma power is phase-locked to theta oscillations in human neocortex. Science 2006;313:1626–8. https://doi.org/10.1126/SCIENCE.1128115. 1979.
[18] Buzsáki G, Draguhn A. Neuronal oscillations in cortical networks. Science 2004;304:1926–9. https://doi.org/10.1126/SCIENCE.1099745. 1979.
[19] Sharott A, McNamara C. OscillTrack – Real-time neuronal oscillation tracking for closed-loop stimulation - ORA. Oxford University Research Archive; 2022. https://doi.org/10.5287/bodleian:qa9ngXrzr.
[20] Xu X, Roby KD, Callaway EM. Immunochemical characterization of inhibitory mouse cortical neurons: three chemically distinct classes of inhibitory cells. J Comp Neurol 2010;518:389–404. https://doi.org/10.1002/CNE.22229.
[21] Gerfen CR, Paletzki R, Heintz N. GENSAT BAC Cre-recombinase driver lines to study the functional organization of cerebral cortical and basal ganglia circuits. Neuron 2013;80:1368–83. https://doi.org/10.1016/J.NEURON.2013.10.016.
[22] Harris JA, Hirokawa KE, Sorensen SA, Gu H, Mills M, Ng LL, et al. Anatomical characterization of Cre driver mice for neural circuit mapping and manipulation. Front Neural Circ 2014;8. https://doi.org/10.3389/FNCIR.2014.00076.
[23] Kozai TDY, Vazquez AL. Photoelectric artefact from optogenetics and imaging on microelectrodes and bioelectronics: New challenges and opportunities. J Mater Chem B 2015;3:4965–78. https://doi.org/10.1039/C5TB00108K.
[24] Kuznetsova A, Brockhoff PB, Christensen RHB. lmerTest package: tests in linear mixed effects models. J Stat Software 2017;82:1–26. https://doi.org/10.18637/JSS.V082.I13.
[25] Owen SF, Liu MH, Kreitzer AC. Thermal constraints on in vivo optogenetic manipulations. Nat Neurosci 2019;22:1061–5. https://doi.org/10.1038/s41593-019-0422-3.
[26] Cardin JA, Carlén M, Meletis K, Knoblich U, Zhang F, Deisseroth K, et al. Driving fast-spiking cells induces gamma rhythm and controls sensory responses. Nature 2009;459:663–7. https://doi.org/10.1038/nature08002.
[27] Sohal VS, Zhang F, Yizhar O, Deisseroth K. Parvalbumin neurons and gamma rhythms enhance cortical circuit performance. Nature 2009;459:698–702. https://doi.org/10.1038/nature07991.
[28] Gunaydin LA, Yizhar O, Berndt A, Sohal VS, Deisseroth K, Hegemann P. Ultrafast optogenetic control. Nat Neurosci 2010;13:387–92. https://doi.org/10.1038/nn.2495.
[29] Adesnik H, Scanziani M. Lateral competition for cortical space by layer-specific horizontal circuits. Nature 2010;464:1155–60. https://doi.org/10.1038/nature08935.
[30] Zou X, Wang DH. On the phase relationship between excitatory and inhibitory neurons in oscillation. Front Comput Neurosci 2016;10:138. https://doi.org/10.3389/FNCOM.2016.00138.
[31] Csicsvari J, Jamieson B, Wise KD, Buzsáki G. Mechanisms of gamma oscillations in the hippocampus of the behaving rat. Neuron 2003;37:311–22. https://doi.org/10.1016/S0896-6273(02)01169-8.
[32] Gulyás AI, Szabó GG, Ulbert I, Holderith N, Monyer H, Erdélyi F, et al. Parvalbumin-containing fast-spiking basket cells generate the field potential oscillations induced by cholinergic receptor activation in the hippocampus. J Neurosci 2010;30:15134–45. https://doi.org/10.1523/JNEUROSCI.4104-10.2010.
[33] Hájos N, Pálhalini J, Mann EO, Nèmeth B, Paulsen O, Freund TF. Spike timing of distinct types of GABAergic interneuron during hippocampal gamma oscillations in vitro. J Neurosci 2004;24:9127–37. https://doi.org/10.1523/JNEUROSCI.2113-04.2004.
[34] Hasenstaub A, Shu Y, Haider B, Kraushaar U, Duque A, McCormick DA. Inhibitory postsynaptic potentials carry synchronized frequency information in active cortical networks. Neuron 2005;47:423–35. https://doi.org/10.1016/j.neuron.2005.06.016.
[35] Canavier CC. Phase-resetting as a tool of information transmission. Curr Opin Neurobiol 2015;31:206–13. https://doi.org/10.1016/J.CONB.2014.12.003.
[36] Hebron H, Lugli B, Dimitrova R, Jaramillo V, Yeh LR, Rhodes E, et al. A closed-loop auditory stimulation approach selectively modulates alpha oscillations and sleep onset dynamics in humans. PLoS Biol 2024;22:e3002651. https://doi.org/10.1371/JOURNAL.PBIO.3002651.
[37] Jaramillo V, Hebron H, Wong S, Atzori G, Bartsch U, Dijk D-J, et al. Closed-loop auditory stimulation targeting alpha and theta oscillations during rapid eye movement sleep induces phase-dependent power and frequency changes. Sleep 2024. https://doi.org/10.1093/SLEEP/ZSAE193. zsae193.
[38] Forger DB. How to shift an oscillator optimally. Biological clocks, rhythms, and oscillations: the theory of biological timekeeping. Cambridge(MA): MIT Press; 2017.
[39] Rudy B, Fishell G, Lee SH, Hjerling-Leffler J. Three groups of interneurons account for nearly 100% of neocortical GABAergic neurons. Dev Neurobiol 2011;71:45–61. https://doi.org/10.1002/DNEU.20853.
[40] Zavala B, Jang A, Trotta M, Lungu CI, Brown P, Zaghloul KA. Cognitive control involves theta power within trials and beta power across trials in the prefrontal-subthalamic network. Brain 2018;141:3361–76. https://doi.org/10.1093/BRAIN/AWY266.
[41] Brier MR, Ferree TC, Maguire MJ, Moore P, Spence J, Tillman GD, et al. Frontal theta and alpha power and coherence changes are modulated by semantic complexity in Go/NoGo tasks. Int J Psychophysiol 2010;78:215–24. https://doi.org/10.1016/J.IJPSYCHO.2010.07.011.
[42] Muthukumaraswamy SD. Functional properties of human primary motor cortex gamma oscillations. J Neurophysiol 2010;104:2873–85. https://doi.org/10.1152/JN.00607.2010.
[43] Nowak M, Hinson E, Van Ede F, Pogosyan A, Guerra A, Quinn A, et al. Driving human motor cortical oscillations leads to behaviorally relevant changes in local

GABAA inhibition: a tACS-TMS study. J Neurosci 2017;37:4481–92. https://doi.org/10.1523/JNEUROSCI.0098-17.2017.

[44] Pfurtscheller G, Lopes Da Silva FH. Event-related EEG/MEG synchronization and desynchronization: basic principles. Clin Neurophysiol 1999;110:1842–57. https://doi.org/10.1016/S1388-2457(99)00141-8.

[45] Stulz SB, Gutkin B, Gilson M, Battaglia D. Phase-dependent stimulation response is shaped by the brain's transient collective dynamics. bioRxiv 2023;2023. https://doi.org/10.1101/2023.05.09.539965. 05.09.539965.

[46] Cardozo Pinto DF, Lammel S. Hot topic in optogenetics: new implications of in vivo tissue heating. Nat Neurosci 2019;22:1039–41. https://doi.org/10.1038/s41593-019-0426-z.

[47] Stujenske JM, Spellman T, Gordon JA. Modeling the spatiotemporal dynamics of light and heat propagation for in vivo optogenetics. Cell Rep 2015;12:525–34. https://doi.org/10.1016/J.CELREP.2015.06.036.

[48] Yizhar O, Fenno LE, Davidson TJ, Mogri M, Deisseroth K. Optogenetics in neural systems. Neuron 2011;71:9–34. https://doi.org/10.1016/J.NEURON.2011.06.004.